

EndoGaussian: Gaussian Splatting for Deformable Surgical Scene Reconstruction

Yifan Liu^{*}, Chenxin Li^{*}, Chen Yang, and Yixuan Yuan (✉)

Chinese University of Hong Kong
{yfliu, chenxinli}@link.cuhk.edu.hk, cyang.ee@my.cityu.edu.hk,
yxyuan@ee.cuhk.edu.hk

Abstract. Reconstructing deformable tissues from endoscopic stereo videos is essential in many downstream surgical applications. However, existing methods suffer from slow inference speed, which greatly limits their practical use. In this paper, we introduce EndoGaussian, a real-time surgical scene reconstruction framework that builds on 3D Gaussian Splatting. Our framework represents dynamic surgical scenes as canonical Gaussians and a time-dependent deformation field, which predicts Gaussian deformations at novel timestamps. Due to the efficient Gaussian representation and parallel rendering pipeline, our framework significantly accelerates the rendering speed compared to previous methods. In addition, we design the deformation field as the combination of a lightweight encoding voxel and an extremely tiny MLP, allowing for efficient Gaussian tracking with a minor rendering burden. Furthermore, we design a holistic Gaussian initialization method to fully leverage the surface distribution prior, achieved by searching informative points from across the input image sequence. Experiments on public endoscope datasets demonstrate that our method can achieve real-time rendering speed (195 FPS real-time, 100× gain) while maintaining the state-of-the-art reconstruction quality (35.925 PSNR) and the fastest training speed (within 2 min/scene), showing significant promise for intraoperative surgery applications. Code is available at: <https://yifliu3.github.io/EndoGaussian/>.

Keywords: 3D Reconstruction · Gaussian Splatting · Robotic Surgery.

1 Introduction

Reconstructing surgical scenes from stereo endoscope videos is crucial to robotic-assisted minimally invasive surgery (RAMIS) [14]. By recovering a 3D model of the observed tissues, such techniques facilitate simulating the surgical environment for preoperative planning and AR/VR medics training [7,11]. Moreover, real-time reconstruction can further expand its applicability to intraoperative use [4,9], empowering surgeons with a complete view of the scene and facilitating their navigation and control of surgical instruments, and potentially paving the way for robotic surgery automation.

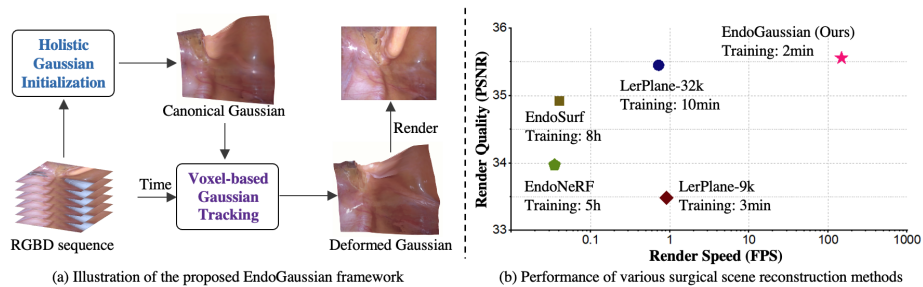


Fig. 1. Illustration of (a) the proposed EndoGaussian framework and (b) performance comparison between our EndoGaussian and previous methods.

Existing efforts [2,12,14,13] for surgical scene reconstruction are based on Neural Radiance Fields (NeRFs), where a network learns a continuous implicit function that maps spatial coordinates to the volumetric density and color. As a pioneer, EndoNeRF [12] represents the dynamic scenes as a canonical field and time-dependent displacement field, achieving an impressive reconstruction effect of deformable tissues. EndoSurf [14] is advanced to use the signed distance field to explicitly constrain the tissue surface, such that the surface reconstruction quality could be improved. Recently, Lerplane [13] further represents dynamic scenes as 4D volumes (3D space and 1D time) and factorizes them into several explicit 2D planes, which greatly alleviates the computation burden and achieves a better trade-off between reconstruction quality and training time. Though the decent reconstruction results of the above methods, these NeRF-based methods are required to repeatedly query the radiance fields at a huge number of points and rays for rendering each view. Consequently, this property greatly limits the rendering speed of these methods, posing great obstacles for the intraoperative rendering systems that necessitate real-time rendering.

Recently, 3D Gaussian Splatting (3DGS) [5] emerged as a promising approach to static scene reconstruction from natural images. It represents the scene as optimizable Gaussians, initialized from Structure-from-Motion (SfM) [10], and renders images by leveraging the efficient splatting. Due to the use of explicit Gaussians and the splatting rendering engine, 3DGS significantly boosts the rendering speed to a real-time level, providing a potential solution for real-time surgical reconstruction. Nevertheless, adopting 3DGS for surgical scenes presents two significant challenges. Firstly, the design of the original 3DGS can not handle the modeling of deformable tissues, yet these dynamic tissues are prevalent during surgical procedures. Secondly, 3DGS relies on SfM to initialize dense Gaussians, while the direct application of SfM to surgical scenes fails to produce accurately initialized points due to the tissue deformation, which violates the underlying assumption of SfM. Therefore, a proper initialization strategy that can work well for the dynamic surgical scene should be delicately designed.

To address these challenges, we propose a novel framework for real-time and high-quality surgical scene reconstruction, named EndoGaussian, by leveraging

the designed Voxel-based Gaussian Tracking and Holistic Gaussian Initialization, as shown in Fig. 1 (a). To model scene dynamics, we design the deformation field as a combination of efficient encoding voxel and an extremely tiny MLP with attribute heads, allowing for Gaussian tracking with a minor rendering burden. Moreover, we achieve the proper initialization of dynamic scenes by re-projecting pixels of a static view into the world coordinates. Considering the points of a single view are limited, we then search points from other views to fulfill a holistic Gaussian initialization. To summarize,

- We propose a real-time and high-quality 4D reconstruction framework, which represents the first effort to use Gaussian Splatting for surgical scene reconstruction with deformable tissues.
- We propose to model scene dynamics with a deformation field, composed of an efficient encoding voxel and an extremely tiny MLP, enabling fast optimization and inference. Moreover, an initialization strategy that can work well under dynamic surgical scenes is designed to correctly leverage the scene distribution prior.
- Extensive benchmarking results in Fig. 1 (b) on surgical scene reconstruction demonstrate our efficacy against prior SOTAs in all aspects, including better rendering efficacy (195 FPS real-time, 100× gain), better rendering quality (35.925 PSNR), and less training overhead (within 2 min/scene), paving the way for real-time intraoperative applications.

2 Method

Our framework is designed for 4D surgical scene reconstruction, by leveraging the recent Gaussian Splatting technique (Sec. 2.1). As shown in Fig. 2, it begins with Holistic Gaussian Initialization to represent the scene as a set of anisotropic Gaussians with corresponding attributes (Sec. 2.2). Then given a query time, we employ the Voxel-based Gaussian Tracking to track the deformation of each Gaussian (Sec. 2.3). After that, differential splatting is used to render the predicted image and depth from deformed Gaussians, from which rendering constraints are calculated to optimize the whole framework (Sec. 2.4).

2.1 Preliminaries

Our work is built upon 3D Gaussian Splatting [5]. It uses a 3D Gaussian representation to model static scenes as they are differentiable and can be easily projected to 2D splats, allowing fast α -blending for image rendering. The 3D Gaussians are defined by the covariance matrix Σ in world space centered at the mean μ , described as $G(\mathbf{x}) = \exp(-1/2(\mathbf{x} - \mu)^T \Sigma^{-1}(\mathbf{x} - \mu))$, where Σ is decomposed into rotation matrix \mathbf{R} and scaling matrix \mathbf{S} . To represent a scene, 3DGS creates a dense set of 3D Gaussians and optimizes their positions μ , rotation \mathbf{R} , scaling \mathbf{S} , opacity o , and their colors, represented by spherical harmonic (SH) coefficients, to capture the view-dependent appearance. These attributes are optimized by rendering the learned Gaussians via a differential splatting, interleaved with steps controlling Gaussian density.

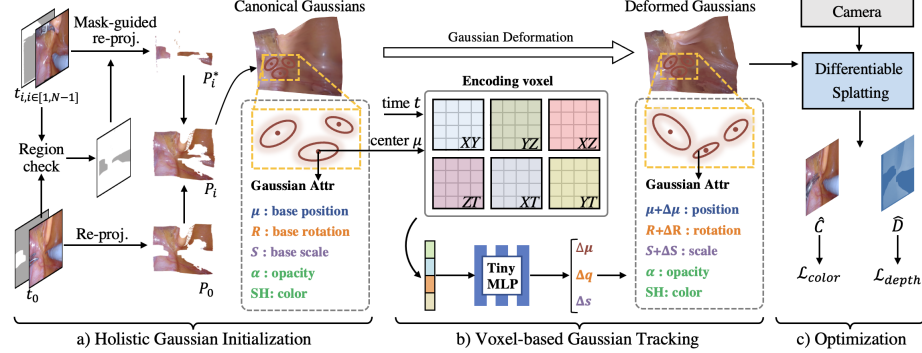


Fig. 2. Illustration of the proposed EndoGaussian framework, which consists of a) Holistic Gaussian Initialization, b) Voxel-based Gaussian Tracking, and c) Optimization.

2.2 Holistic Gaussian Initialization

Given an image sequence $\{\mathbf{I}_i, \mathbf{D}_i, \mathbf{M}_i\}_{i=0}^{T-1}$ composed of image $\mathbf{I}_i \in \mathbb{R}^{H \times W \times 3}$, depth $\mathbf{D}_i \in \mathbb{R}^{H \times W}$, and tool occlusion mask $\mathbf{M}_i \in \{0, 1\}^{H \times W}$, where 0 and 1 denotes tools and tissues respectively, Gaussian initialization aims to generate dense and accurate initialized points $\mathbf{P} \in \mathbb{R}^{N \times 3}$ with Gaussian attributes.

One feasible approach is to re-project pixels of the canonical view \mathbf{I}_0 into the world coordinates to obtain the initialized points \mathbf{P}_0 :

$$\mathbf{P}_0 = \mathbf{D}_0 \mathbf{K}^{-1} \mathbf{T}_0 (\mathbf{I}_0 \circ \mathbf{M}_0), \quad (1)$$

where \mathbf{M}_0 is used to filter our tool pixels as we desire reconstruction of the underlying tissues, \mathbf{K} and \mathbf{T}_0 refers to the camera intrinsic and extrinsic matrix. Though effective, such an initialization strategy suffers from incomplete points caused by the limited view and occlusions of tool masks, as shown in Fig. 2 (a). This problem can be solved by searching points from other views, since more views would perceive more points and the regions that are occluded by the tool in \mathbf{I}_0 , can be visible in another view due to the tool movement. Therefore, we iteratively re-project pixels of other views \mathbf{I}_i into the world coordinates \mathbf{P}_i similarly as Eq. 1, and find those points that fall into the tool region in \mathbf{I}_0 or fall into the outside of image \mathbf{I}_0 :

$$\mathbf{P}_i^* = \{\mathbf{p}_j \in \mathbf{P}_i | \mathbf{K} \mathbf{T}_i^{-1} \mathbf{p}_j \notin \text{coords}(\mathbf{I}_0) \text{ or } \mathbf{K} \mathbf{T}_i^{-1} \mathbf{p}_j \in \text{coords}(\mathbf{M}_0)\}, \quad (2)$$

where $\text{coords}(\mathbf{I}_0)$ refers to the coordinates of the canonical view \mathbf{I}_0 , and $\text{coords}(\mathbf{M}_0)$ denotes the coordinates of the tool pixels. After that, we combine the processed \mathbf{P}_i^* with \mathbf{P}_0 to form a more complete points: $\mathbf{P} = \text{concat}(\mathbf{P}_i^*, \mathbf{P}_0)$, $i \in [1, T-1]$, where T is the length of the input image sequence. By performing the above operation across input views, a rather complete point cloud can be obtained as a beneficial initialization, since Gaussian Splatting relies on the quantity and the

quality of initialized points to perform fast optimization. Based on the initialized points \mathbf{P} , a static scene can be represented as a dense set of 3D Gaussians $\mathbf{G}_0 = \{(\boldsymbol{\mu}_i, \mathbf{R}_i, \mathbf{S}_i, \alpha, SH_i)\}_{i=1}^N$, where $\boldsymbol{\mu}_i = \mathbf{p}_i$, $\mathbf{p}_i \in \mathbf{P}$, and other attributes are randomly initialized.

2.3 Voxel-based Gaussian Tracking

To model surface dynamics, we represent the deformable surgical scene as canonical Gaussians \mathbf{G}_0 and a deformation field \mathbf{D} , from which the deformed Gaussians \mathbf{G}_t can be calculated to render images at query time t . Canonical Gaussians \mathbf{G}_0 can be initialized by the method described in Sec. 2.2, while an efficient deformation field should also be carefully designed. Naively using large neural networks to track the deformation would incur slow inference speed due to the computational burden, thus we decompose the deformation field into two lightweight modules $\mathbf{D} = \mathbf{F} \circ \mathbf{E}$, where \mathbf{E} is a 4D encoding voxel and \mathbf{F} represents an extremely tiny MLP with attribute heads.

4D encoding voxel The encoding voxel \mathbf{E} is used to encode the 4D inputs, i.e., the center of Gaussian $\boldsymbol{\mu} = (x, y, z)$ and the query time t , into the latent feature \mathbf{f} . Considering the efficiency need, we decompose the 4D encoding voxel as six discrete planes with corresponding vectors, inspired by [3]:

$$\mathbf{E} = \mathbf{E}^{\mathbf{XY}} \otimes \mathbf{E}^{\mathbf{ZT}} \otimes \mathbf{v}^1 + \mathbf{E}^{\mathbf{XY}} \otimes \mathbf{E}^{\mathbf{ZT}} \otimes \mathbf{v}^2 + \mathbf{E}^{\mathbf{XY}} \otimes \mathbf{E}^{\mathbf{ZT}} \otimes \mathbf{v}^3, \quad (3)$$

where \otimes refers to the outer product, $\mathbf{E}^{\mathbf{AB}} \in \mathbb{R}^{\mathbf{AB}}$ is a learned plane of features, and $\mathbf{v}^i \in \mathbb{R}^{\mathbb{D}}$ denotes the feature vector along i -th axis. To query a latent feature \mathbf{f} given the continuous inputs (x, y, z, t) , we project the 4D coordinates onto the decomposed 2D planes and utilize the bilinear interpolation to obtain the latent feature \mathbf{f} . Through the decomposition in Eq. 3, the computational cost is reduced from $\mathcal{O}(N^3)$ to $\mathcal{O}(N^2)$, which leads to a considerable acceleration of training and rendering period.

Tiny MLP with attribute heads When the all information of 3D Gaussians is encoded, we can compute any desired variable with a tiny encoder. Therefore, a compact decoder layer \mathbf{F} proves to be sufficient for decoding and merging all the necessary information. Finally, separate attribute heads are employed to compute the deformation of position $\Delta\boldsymbol{\mu}$, rotation $\Delta\mathbf{R}$, and scaling $\Delta\mathbf{S}$,

$$\Delta\boldsymbol{\mu}, \Delta\mathbf{R}, \Delta\mathbf{S} = \mathbf{F}(\mathbf{f}). \quad (4)$$

Then, the attributes of deformed Gaussians \mathbf{G}_t can be computed as:

$$(\boldsymbol{\mu}', \mathbf{R}', \mathbf{S}', o', SH') = (\boldsymbol{\mu} + \Delta\boldsymbol{\mu}, \mathbf{R} + \Delta\mathbf{R}, \mathbf{S} + \Delta\mathbf{S}, o, SH), \quad (5)$$

where the deformation of opacity and the SH coefficients are not modeled, since we empirically find that modeling the position and covariance deformation is sufficient enough to capture the tissue movement and shape variations.

2.4 Optimization

Splatting-based rendering. Given deformed Gaussians $\mathbf{G}_t = \{\boldsymbol{\mu}, \mathbf{R}, \mathbf{S}, o, SH\}$ at query time t , we order all the Gaussians that contributes to a pixel \mathbf{x} to render colors and depths using the following function [5] :

$$\hat{\mathbf{C}}(\mathbf{x}) = \sum_{i=1}^n \mathbf{c}_i \alpha_i \prod_{j=1}^{i-1} (1 - \alpha_j), \quad \hat{\mathbf{D}}(\mathbf{x}) = \sum_{i=1}^n d_i \alpha_i \prod_{j=1}^{i-1} (1 - \alpha_j), \quad (6)$$

where \mathbf{c}_i is the color computed from the SH coefficients of i -th Gaussian, d_i denotes the z-buffer of the i -th Gaussian, and α_i is given by evaluating a projected 2D covariance matrix $\boldsymbol{\Sigma}'_i$ multiplied by the opacity o_i . The 2D covariance matrix is calculated by $\boldsymbol{\Sigma}' = \mathbf{J}\mathbf{W}\boldsymbol{\Sigma}\mathbf{W}^T\mathbf{J}^T$, $\boldsymbol{\Sigma} = \mathbf{R}\mathbf{S}\mathbf{S}^T\mathbf{R}^T$, where \mathbf{J} denotes the Jacobian of the affine approximation of the projective transformation, and \mathbf{W} is the view transformation matrix.

Loss. We train the network to minimize the difference between the actual and rendered results by the rendering constraint $\mathcal{L} = (\lambda_1\mathcal{L}_{color} + \lambda_2\mathcal{L}_{depth})$, where $\lambda_{i=1,2}$ are balancing weights. \mathcal{L}_{color} and \mathcal{L}_{depth} are the color and depth reconstruction losses respectively, and they are defined as:

$$\mathcal{L}_{color} = \sum_{\mathbf{x} \in \mathcal{I}} \|\mathbf{M}(\mathbf{x})(\hat{\mathbf{C}}(\mathbf{x}) - \mathbf{C}(\mathbf{x}))\|_1, \quad \mathcal{L}_{depth} = \sum_{\mathbf{x} \in \mathcal{I}} \|\mathbf{M}(\mathbf{x})(\hat{\mathbf{D}}(\mathbf{x}) - \mathbf{D}(\mathbf{x}))\|_1, \quad (7)$$

where \mathbf{M} , $\{\hat{\mathbf{C}}, \hat{\mathbf{D}}\}$, $\{\mathbf{C}, \mathbf{D}\}$, and \mathcal{I} are binary tool masks, predicted colors and depths, real colors and depths, and 2D coordinate space.

3 Experiments

3.1 Experiment settings

Datasets and evaluation We conduct experiments on two publicly available datasets, ENDONERF [12] and SCARED [1]. ENDONERF [12] contains two cases of in-vivo prostatectomy data, which is captured from stereo cameras at a single viewpoint and encompasses challenging scenes with non-rigid deformation and tool occlusion. SCARED [1] collects the ground truth RGBD images of five porcine cadaver abdominal anatomies, using a DaVinci endoscope and a projector. Following previous work [14], we split the frame data of each scene into 7:1 training and testing sets. We evaluate our method by comparing it with recent surgical scene reconstruction methods [12,14,13] using standard image quality metrics as in [14], including PSNR, SSIM, and LPIPS. Additionally, to measure the training efficiency and rendering speed, we record the optimization time during training and Frames-Per-Second (FPS) during inference.

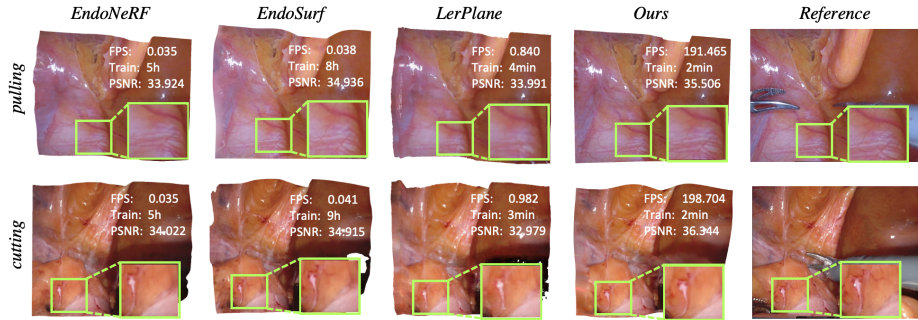


Fig. 3. Illustration of the rendered images of previous works and ours.

Implementation details In the initialization stage, we randomly sample 0.1% points to reduce the redundancy. The encoding voxel size is set as [64, 64, 64, 100] for the length, width, height, time, and the network width of the tiny MLP is 32. To optimize Gaussians and the deformation field, we use Adam [6] as the optimizer with an initial learning rate 1.6×10^{-3} . We employ a warmup strategy, where the canonical Gaussians are first optimized for 1k iterations, and then the whole framework is optimized for 3k iterations. The training of the framework takes around 2 minutes on a single RTX 4090 GPU running Ubuntu 22.04. Our EndoGaussian is implemented with pure Pytorch [8].

3.2 Main results

We compare our proposed method against existing SOTA reconstruction methods: EndoNeRF [12], EndoSurf [14], and LerPlane [13]. As shown in Tab. 1, we observe that EndoNeRF and EndoSurf achieve high-quality reconstruction of deformed tissues but require hours for optimization, which is quite computationally expensive. In contrast, LerPlane greatly accelerates the training process to only around 3 minutes, yet compromises the reconstruction performance. More iterations can promote the rendering quality of LerPlane, but it still suffers from extremely slow inference speed. Our method EndoGaussian, on the other hand, achieves state-of-the-art reconstruction results using only 2 minutes on the ENDONERF dataset, and most importantly, achieves real-time rendering of 195 FPS, providing more than $100\times$ acceleration over existing methods. In addition, we illustrate several qualitative results in Fig. 3. It can be observed that our method can preserve more details and provide better visualizations of the deformable tissues compared to other methods. These results demonstrate that EndoGaussian achieves real-time and high-quality surgical scene reconstructions, showing significant promise for future intraoperative applications.

3.3 Ablation Study

Gaussian Initialization We experiment with ‘random’ initialization that randomly generates initialized points and ‘single’ initialization that re-projects pix-

Table 1. Performance comparison on the ENDONERF [12] and SCARED [1] dataset.

Dataset	Method	PSNR \uparrow	SSIM \uparrow	LPIPS \downarrow	TrTime \downarrow	FPS \uparrow
ENDONERF	EndoNeRF [12]	33.973	0.933	0.156	5 hours	0.035
	EndoSurf [14]	34.926	<u>0.954</u>	0.113	8.5 hours	0.040
	LerPlane-9k [13]	33.485	0.926	0.146	<u>3.5 min</u>	<u>0.911</u>
	LerPlane-32k [13]	<u>35.380</u>	0.950	<u>0.102</u>	8.5 min	0.872
	EndoGaussian (Ours)	35.925	0.958	0.096	2 min	195.085
SCARED	EndoNeRF [12]	22.867	0.768	0.382	3.5 hours	0.016
	EndoSurf [14]	23.566	0.802	0.350	5.8 hours	0.009
	LerPlane-9k [13]	22.565	0.738	0.421	<u>3 min</u>	<u>0.815</u>
	LerPlane-32k [13]	<u>24.128</u>	<u>0.817</u>	<u>0.306</u>	7 min	0.792
	EndoGaussian (Ours)	26.619	0.840	0.287	2.5 min	117.135

Table 2. Ablation study of the designed components on ENDONERF [12].

Component	Method	PSNR \uparrow	SSIM \uparrow	LPIPS \downarrow	TrTime \downarrow	FPS \uparrow
Gaussian initialization	random	6.023	0.282	0.604	2min	197.776
	single	35.201	0.952	1.065	2min	185.813
	ours	35.925	0.958	0.096	2min	195.085
Deformation model	MLP	33.301	0.938	0.137	9 min	144.319
	ours	35.925	0.958	0.096	2 min	195.085

els of the canonical view into the world coordinates. From Tab. 2, we observe that ‘random’ can hinder model optimization and lead to poor reconstruction results, while reconstruction results of ‘single’ are often compromised due to the obstruction caused by surgical tools. In contrast, our initialization method can avoid these problems, leading to a better reconstruction quality.

Deformation model The 4D encoding voxel can retain 3D Gaussians’ spatial-temporal information with minor optimization and rendering burden. As shown in Tab. 2, replacing it with MLP falls short in modeling complex deformations across various settings, and decreases the optimization and rendering speed.

4 Conclusion

In this paper, we propose a real-time and high-quality 4D reconstruction framework for dynamic surgical scene reconstruction. By utilizing Voxel-based Gaussian Tracking and Holistic Gaussian Initialization, we can handle tissue deformation and non-trivial Gaussian initialization problems. Comprehensive experiments show that our EndoGaussian can achieve state-of-the-art reconstruction quality with real-time rendering speed, which is over $100\times$ faster than previous methods. We hope the emerging Gaussian Splatting-based reconstruction techniques could inspire new pathways for robotic surgery scene understanding, and empower various downstream clinical tasks, especially intraoperative applications.

References

1. Allan, M., Mcleod, J., Wang, C., Rosenthal, J.C., Hu, Z., Gard, N., Eisert, P., Fu, K.X., Zeffiro, T., Xia, W., et al.: Stereo correspondence and reconstruction of endoscopic data challenge. arXiv preprint arXiv:2101.01133 (2021)
2. Battle, V.M., Montiel, J.M., Fua, P., Tardós, J.D.: Lightneus: Neural surface reconstruction in endoscopy using illumination decline. In: International Conference on Medical Image Computing and Computer-Assisted Intervention. pp. 502–512. Springer (2023)
3. Cao, A., Johnson, J.: Hexplane: A fast representation for dynamic scenes. In: Proceedings of the IEEE/CVF Conference on Computer Vision and Pattern Recognition. pp. 130–141 (2023)
4. Chen, L., Tang, W., John, N.W., Wan, T.R., Zhang, J.J.: Slam-based dense surface reconstruction in monocular minimally invasive surgery and its application to augmented reality. *Computer methods and programs in biomedicine* **158**, 135–146 (2018)
5. Kerbl, B., Kopanas, G., Leimkühler, T., Drettakis, G.: 3d gaussian splatting for real-time radiance field rendering. *ACM Transactions on Graphics* **42**(4) (2023)
6. Kingma, D.P., Ba, J.: Adam: A method for stochastic optimization. arXiv preprint arXiv:1412.6980 (2014)
7. Liu, X., Stiber, M., Huang, J., Ishii, M., Hager, G.D., Taylor, R.H., Unberath, M.: Reconstructing sinus anatomy from endoscopic video—towards a radiation-free approach for quantitative longitudinal assessment. In: Medical Image Computing and Computer Assisted Intervention—MICCAI 2020: 23rd International Conference, Lima, Peru, October 4–8, 2020, Proceedings, Part III 23. pp. 3–13. Springer (2020)
8. Paszke, A., Gross, S., Chintala, S., Chanan, G., Yang, E., DeVito, Z., Lin, Z., Desmaison, A., Antiga, L., Lerer, A.: Automatic differentiation in pytorch (2017)
9. Penza, V., De Momi, E., Enayati, N., Chupin, T., Ortiz, J., Mattos, L.S.: Envisors: Enhanced vision system for robotic surgery. a user-defined safety volume tracking to minimize the risk of intraoperative bleeding. *Frontiers in Robotics and AI* **4**, 15 (2017)
10. Schonberger, J.L., Frahm, J.M.: Structure-from-motion revisited. In: Proceedings of the IEEE conference on computer vision and pattern recognition. pp. 4104–4113 (2016)
11. Tang, R., Ma, L.F., Rong, Z.X., Li, M.D., Zeng, J.P., Wang, X.D., Liao, H.E., Dong, J.H.: Augmented reality technology for preoperative planning and intraoperative navigation during hepatobiliary surgery: A review of current methods. *Hepatobiliary & Pancreatic Diseases International* **17**(2), 101–112 (2018)
12. Wang, Y., Long, Y., Fan, S.H., Dou, Q.: Neural rendering for stereo 3d reconstruction of deformable tissues in robotic surgery. In: International Conference on Medical Image Computing and Computer-Assisted Intervention. pp. 431–441. Springer (2022)
13. Yang, C., Wang, K., Wang, Y., Yang, X., Shen, W.: Neural lerplane representations for fast 4d reconstruction of deformable tissues. arXiv preprint arXiv:2305.19906 (2023)
14. Zha, R., Cheng, X., Li, H., Harandi, M., Ge, Z.: Endosurf: Neural surface reconstruction of deformable tissues with stereo endoscope videos. In: International Conference on Medical Image Computing and Computer-Assisted Intervention. pp. 13–23. Springer (2023)